第 52 卷第 6 期
2024 年 6 月

硅 酸 盐 学 报
JOURNAL OF THE CHINESE CERAMIC SOCIETY

Vol. 52，No. 6
June，2024

http://www.gxyb.cbpt.cnki.net

DOI：10.14062/j.issn.0454-5648.20230821

熔融沉积方法增材制造锆钛酸铅压电陶瓷

刘月明[1]，董浩霖[1]，刘 鹏[1]，杨现锋[1]，赵 巍[2]，谢志鹏[3]

(1. 长沙理工大学材料科学与工程学院，长沙 410114; 2. 天津城建大学材料科学与工程学院，天津 300384;
3. 清华大学，新型陶瓷与精细工艺国家重点实验室，北京 100083)

摘 要：采用基于螺杆挤出的熔融沉积成型方法结合两步脱脂工艺增材制造了 PZT 压电陶瓷，研究了固相含量对耗材流变性质、密度和收缩率的影响，以 87%(质量分数)耗材为主，观察了显微形貌并测试了电学性能。结果表明，制备的高固相低黏度打印混合料呈现典型的剪切变稀流变学性质，具有优异的打印性能，成功打印了壁厚 1 mm 的环形阵列、阵元间距为 0.25 mm 的矩形阵列和 30°倾角的环形薄壁生坯样品，且 PZT 陶瓷样品层间结合良好，成功制备了无支撑球壳结构的 PZT 陶瓷样品。随着固相含量的增加，PZT 陶瓷的密度随之升高，固相含量为 87%时，PZT 陶瓷的密度为 7.82 g/cm^3，压电常数 d_{33} 达到 316 pC/N，为制备复杂结构的 PZT 压电陶瓷提供了新的思路。

关键词：3D 打印；锆钛酸铅；熔融沉积成型；压电陶瓷
中图分类号：TM282 **文献标志码**：A **文章编号**：0454–5648(2024)06–1953–09
网络出版时间：2024–05–22

压电陶瓷是一种能将机械能和电能互相转换的功能陶瓷材料。由于具有较好的力学性能和稳定的压电性能，已经在传感器、超声换能器、微位移器和其它电子元器件等方面得到了广泛的应用[1–5]。其中应用最多的材料之一是锆钛酸铅(PZT)，由于其优良的压电特性和稳定性，它已成为航空航天、武器装备和超声波成像的首选材料[6–10]。由于高端技术领域对压电功能器件智能化、集成化、轻量化的发展需求，压电陶瓷的外形和结构越来越复杂。传统的压电陶瓷制造工艺，大多需借助模具或刀具完成[11]，很难甚至无法制造具有中空、悬垂等复杂结构的压电陶瓷，制约了压电功能器件的进一步发展[12]。

与传统成型技术相比，增材制造技术的最大优势在于无需模具即可实现外形复杂的部件快速成型，这与多样化的压电陶瓷及其器件研发需求十分契合，同时因其样品后续加工量少、原材料利用率高、无需切削液的特点，得到了学术界和工业界的广泛关注[13–14]。在陶瓷材料增材制造领域，功能陶瓷和器件的研究仍在增长期。目前常用的压电陶瓷增材制造工艺根据所用原材料的不同形态可分为：1)基于粉体的增材制造工艺：激光选区烧结(SLS)[15]、黏结剂喷射(BJ)[16]等；2)基于浆料的增材制造工艺：立体光刻(SLA)[17–18]、数字光处理(DLP)[19]、墨水喷射(IJP)[16]、墨水直写(DIW)[20]等; 3)基于块材的增材制造工艺：熔融沉积(FDM)[21]、薄材叠层(LOM)[22]等。在这些增材制造技术中，由于陶瓷粉末熔点高，SLS 要获得表面质量高、尺寸精度高的致密材料较难[23]；SLA 和 DLP 以微米级的打印精度被重点关注，但压电陶瓷粉体通常密度较大、折射率较高，与树脂混合成悬浮液后不稳定，容易产生沉降，光固化成型有难度[24]；LOM 制备的陶瓷材料致密度相对较高，然而对耗材的利用率不高[25]；DIW 成本较低，陶瓷粉体适用性高，但坯体力学强度较差，打印过程中容易发生形变或者收缩引起的开裂[26]。

熔融沉积成型技术(FDM)使用将陶瓷粉体和热熔性有机黏结剂等助剂混合而成的颗粒耗材，将颗粒在略高于熔点的环境温度下熔化成流体状，接着在计算机控制下逐步挤出并沉积到下方的载体上，进而逐层叠加成型。相较于粉体及浆料，FDM 技术

收稿日期：2023–10–25。 修订日期：2023–12–27。
基金项目：国家自然科学基金(52172063)；湖南省研究生科研创新项目(CX20210830)。
第一作者：刘月明(1998—)，男，硕士研究生。
通信作者：杨现锋(1980—)，男，博士，教授。

Received date: 2023–10–25. **Revised date:** 2023–12–27.
First author: LIU Yueming (1998–), male, Master candidate.
E-mail: liuyueming1998@foxmail.com
Correspondent author: YANG Xianfeng(1980–), Male, Ph.D., Professor.
E-mail: yangxfcsust@csust.edu.cn

更具灵活性，且基于颗粒的打印耗材，省略了丝材制备过程[27–29]。近年来，利用 FDM 制备 PZT 陶瓷材料的研究较少，在压电领域主要用于制备压电复合材料。如用于传感器的 PZT-5H 陶瓷/环氧 2–2 复合材料[30]、PVDF 用于制备活性压电层[31]、MWCNT/BT/PVDF 纳米复合薄膜用于传感器[32]、用于制备三维压电纳米复合材料晶格的 PZT/TPU 压电纳米复合材料[33]，但采用 FDM 制备纯 PZT 压电陶瓷的研究却较少被报道。

本研究采用熔融沉积成型(FDM)结合螺杆挤出结合两步脱脂工艺的方法，以 PZT 粉体和有机物黏结剂为主要原料，研究了打印耗材的流变性质，研究了固相含量对 PZT 烧结样品密度和收缩率的影响，以 87%(质量分数)的打印耗材为主，打印了不同形状的试样，脱脂烧结后制备了性能较为稳定的 PZT 压电陶瓷。为 FDM 制备压电陶瓷提供了参考，丰富了压电陶瓷复杂构件的制备技术。

1 实验

1.1 原材料

主要原料为锆钛酸铅粉体(PZT, d_{50} =2.85 μm，中国电子科技集团有限公司第四十六研究所)，图 1 为 PZT 粉体的 X 射线衍射谱以及显微形貌。由图 1a 可见，PZT 粉体的锆钛摩尔比为 52:48。黏结剂包括石蜡(PW, 99%, 纯度，后同)、硬脂酸(SA, 98%)、聚乙烯(PE, 99%)、和乙烯–醋酸乙烯共聚物(EVA, 98%)，PZT 耗材中有机物的质量比为 *m*(PW): *m*(SA): *m*(PE): *m*(EVA) = 58:5:20:17。

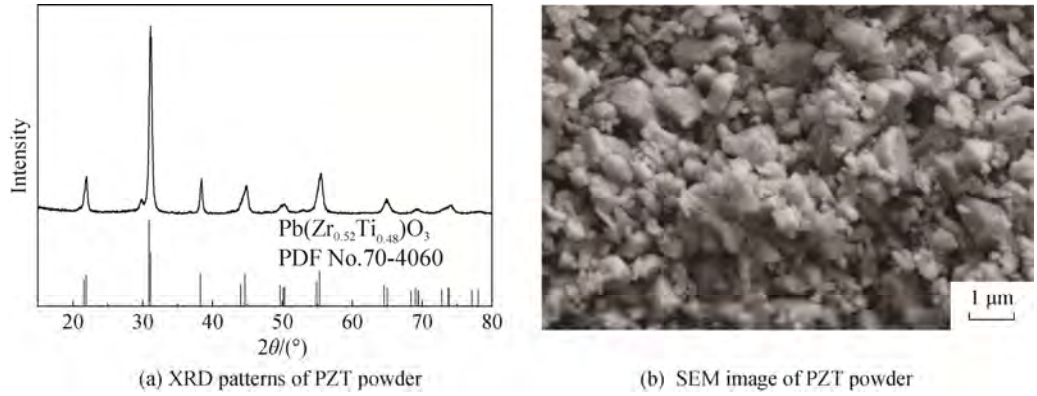

(a) XRD patterns of PZT powder (b) SEM image of PZT powder

图 1 PZT 粉体 XRD 谱与微观形貌 SEM 照片

Fig. 1 XRD pattern and SEM image of PZT powder

1.2 打印成型与烧结

图 2 为熔融沉积成型法(FDM)制备 PZT 陶瓷的工艺流程图。由图 2 可见，锆钛酸铅粉体与黏结剂于 130 ℃在双辊机上混合均匀，冷却破碎至直 5 mm 左右的颗粒，获得用于熔融沉积成型的打印耗材。使用螺杆挤出 FDM 打印机(UP-R200，深圳升华三维科技有限公司)打印生坯。工艺参数：打印层厚为 0.2 mm；喷嘴直径为 0.5 mm；挤出料筒温度为 120 ℃；打印速率为 40 mm·s^{-1}；打印平台温度为 85 ℃。采用单线路径打印出圆片生坯(ϕ=25 mm，h=3 mm)与其他不同尺寸的异形件。

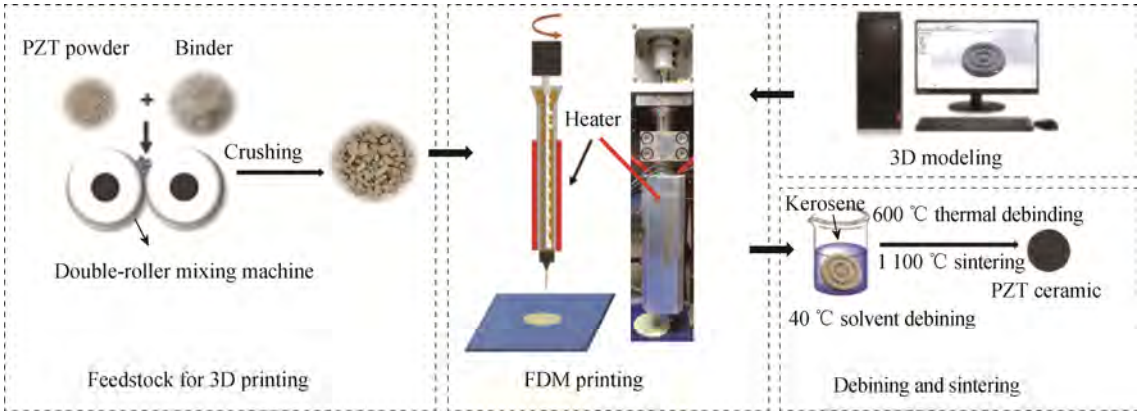

图 2 PZT 陶瓷的 FDM 制备工艺原理图

Fig. 2 Schematic diagram of the FDM preparation process of PZT ceramics

打印坯体先放入 40 ℃煤油中浸泡 20 h 进行溶剂脱脂，取出置于 40 ℃烘箱中干燥 15 h，随后进行高温脱脂，从室温升温至 600 ℃保温 2 h 以完全排出有机物。热脱脂后的样品放入带盖坩埚中，埋入 PZT 粉中，升至 1 100 ℃保温 2 h。

1.3　被银与极化

将圆片样品正反表面进行打磨后，先在样品正面涂上导电银浆，放入 120 ℃鼓风干燥箱 20 min 后取出，对另一面进行相同处理。随后放入管式炉中，以 5 ℃/min 的升温至 720 ℃，保温 30 min，随炉冷却，磨去侧面多余银层；将样品置于 120 ℃硅油中，在 2.5 kV/mm 的直流电场下极化 20 min，取出冷却擦拭后用放电夹放电。

1.4　样品表征

采用 X 射线衍射仪(XRD, D8 Advance, German)测试物相结构。使用毛细管流变仪(Rosand RH2000, Malvern, UK)在 180 ℃测试了打印耗材的流变性质。采用场发射扫描电子显微镜(SEM, JSM-6700F, JEOL, Japan)观察样品的微观形貌。用排水法测量了样品密度。采用阻抗分析仪(Agilent-4294A, USA)测量了样品的电容和介电损耗。采用铁电测试仪(德国-aix ACCT-TF Analyzer 2000)分析了样品的铁电性能。采用准静态 d_{33} 测量仪(ZJ-3AN, 北京精科智创科技发展有限公司)测量了样品的压电常数 d_{33}。

2　结果与讨论

2.1　PZT 耗材打印性能评价

配制了 4 种固相含量的 PZT 打印耗材。PW 能提供良好的流动性；SA 可作为表面活性剂促进陶瓷粉体与有机物的结合；PE 熔点高，能够提高耗材的塑性；EVA 具有较低的熔点及黏度。

图 3 为打印耗材的剪切黏度剪切速率曲线。由图 3 可见，当固相含量一定时，剪切黏度随着剪切速率的增加而减小，具有明显的剪切变稀特性，这使得耗材在被挤出的过程中黏度较小，有利于耗材的顺利挤出；当剪切速率一定时，固相含量越高，测得的剪切黏度也越高，如剪切速率为 100 s^{-1} 时，随着固相含量的增加，剪切黏度分别为 30.30、45.07、47.08 Pa·s 和 655.21 Pa·s，一方面是因为体系内起到促进流动的有机物黏结剂组分减少；另一方面 PZT 粉体颗粒间的接触几率增大，移动的阻力随之增大。当固相含量为 83%时，耗材内的有机物黏结剂含量较多，随着剪切速率的增加，仅测至 300 s^{-1} 的剪切黏度，剪切速率进一步增加会使得剪切黏度低于毛细管流变仪的黏度测试下限；固相含量为 85%和 87%时，测得的剪切黏度较为稳定；当固相含量为 89%时，测得的剪切黏度明显增加。

图 4 为颗粒状 PZT 打印耗材与挤出状态实物图。之后实验主要选用固相含量为 87%的 PZT 打印耗材。

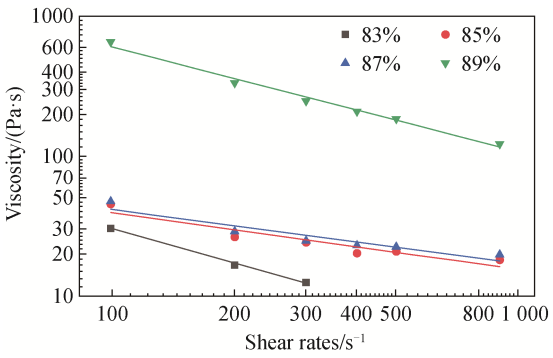

图 3　打印耗材的剪切黏度–剪切速率曲线

Fig. 3　Shear viscosity *vs.* shear rate curve of the feedstock with different solid loading

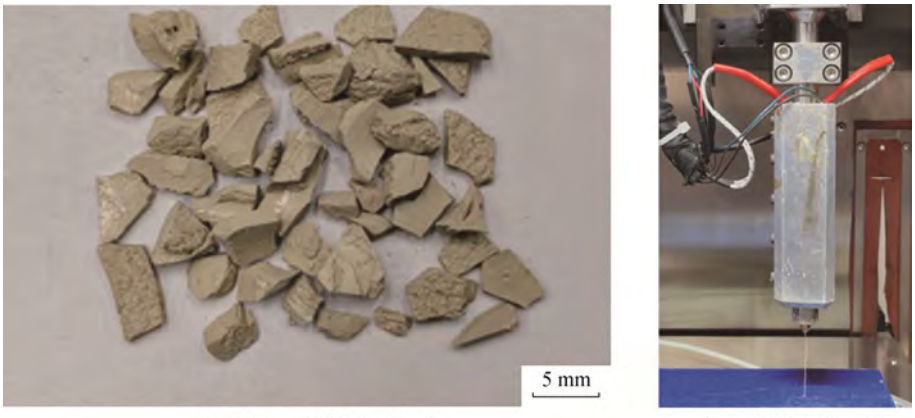

(a) Pellets of PZT feedstock　　(b) Extruded filament

图 4　PZT 耗材颗粒与挤出状态

Fig. 4　Pellets of PZT feedstock and extruded filament

图 5 为 87%PZT 耗材打印制备的生坯样品实物照片，分别为环形阵列(图 5a)、矩形阵列(图 5b)与不同倾角的环形薄壁结构(图 5c)。由图 5a~图 5c 可见，最薄实现了壁厚 1 mm 的环形阵元生坯打印；矩形阵列方面，打印了阵元间距最低为 0.25 mm 的矩形阵列；环形薄壁方面，打印了高 20 mm、壁厚 1.5 mm 的环形薄壁结构，实现了 90°到 30°倾角薄壁结构的打印，说明制备的 PZT 耗材具有良好的打印性能。

2.2 层间结合与显微形貌

图 6 为 PZT 打印坯体和烧结体的微观形貌。由图 6a 可见，固相含量为 87%的打印生坯样品层间结合表面的显微形貌呈现 FDM 工艺典型表面台阶特征，结合图 6b 和图 6c 可知，生坯样品表面台阶的深度约 80 μm，层间厚度约 200 μm，烧结样品表面台阶的深度约 72 μm，层间厚度约 150 μm，表面的台阶间隙未延伸至坯体内部。由图 6d、图 6e 和图 6f 可以看出，经过脱脂和烧结后样品发生收缩，层厚降低，断面内部均匀致密且无明显孔隙缺陷，说明熔融沉积法 3D 打印可以制备出层间结合良好的 PZT 陶瓷。

图 7 为 4 种固相含量的 PZT 打印生坯与经 1 100 ℃烧结 2 h 制备的烧结样品的密度。由图 7 可见，打印生坯和烧结样品的密度都随着固相含量的增加而增加，其中烧结件的密度由 7.55 g/cm^3 上升至 7.84 g/cm^3，低于压制样品的 7.94 g/cm^3。随着固相含量的增加，PZT 陶瓷粉体含量增加，耗材内部的有机物黏结剂减少，且 PZT 粉体的密度大于有机物黏结剂的密度，所以生坯密度逐渐增加，而烧结样品排出了内部的有机物黏结剂，结构进一步致密化，较生坯样品密度增大。

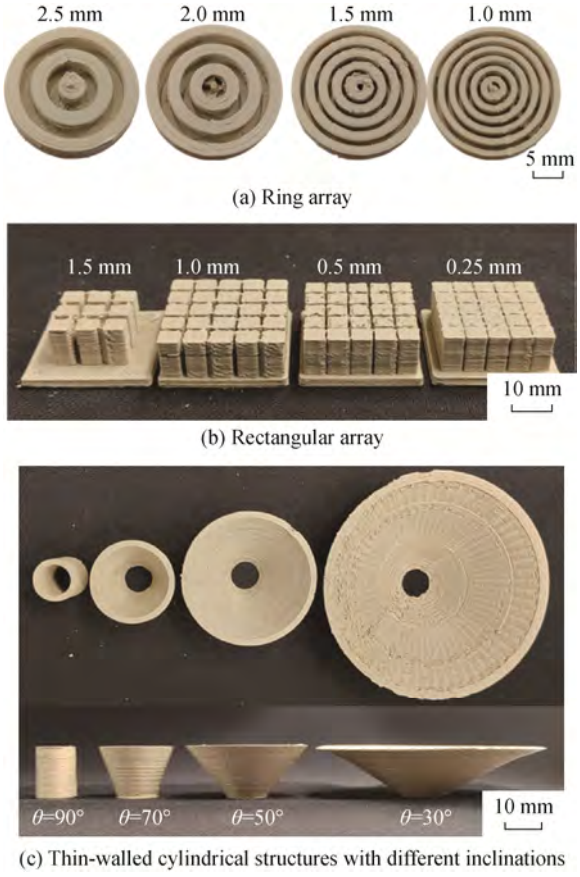

图 5 FDM 制备的 PZT 实物生坯

Fig. 5 Images of PZT ceramic green bodies prepared by FDM

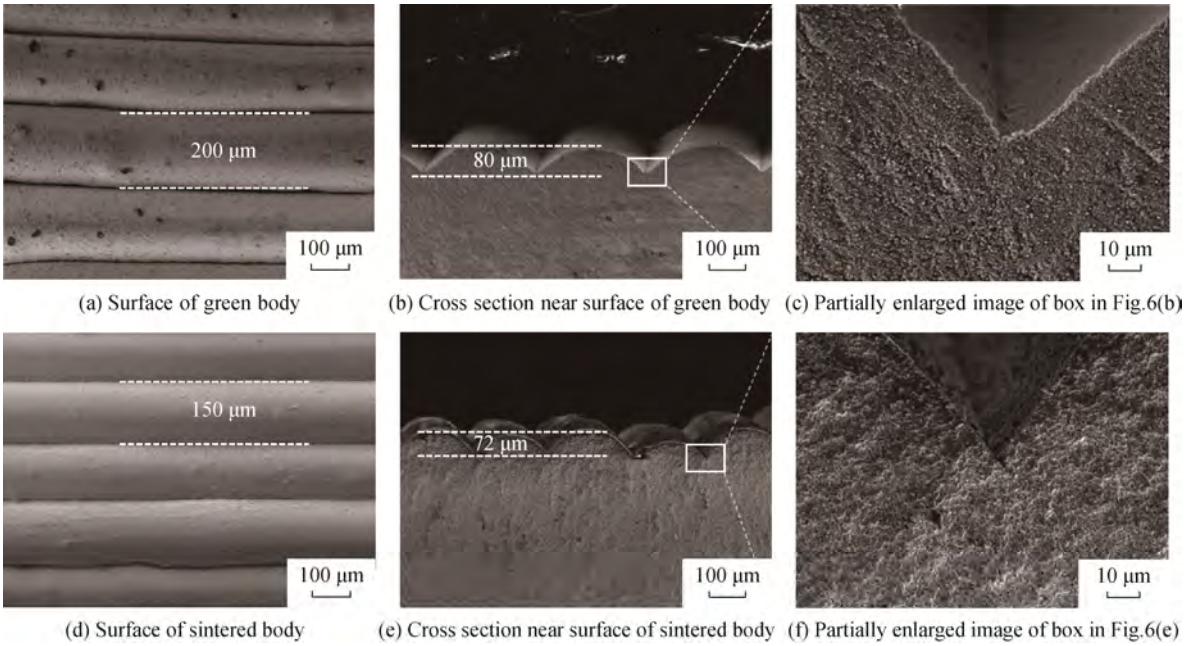

图 6 PZT 打印坯体和烧结体的 SEM 照片

Fig. 6 SEM images of PZT green body and sintered body

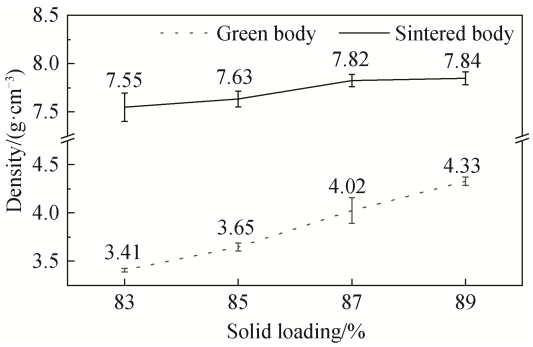

图 7　不同固相含量的生坯样品与烧结样品密度

Fig. 7　Density of green bodies and sintered bodies

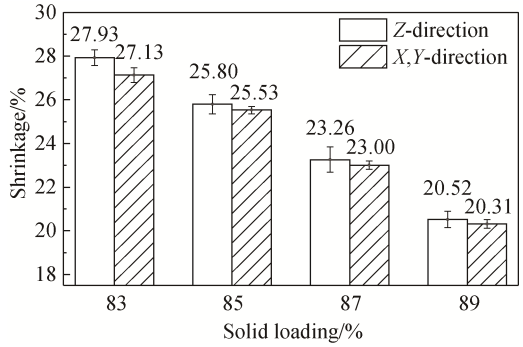

图 8　不同固相含量坯体 *Z* 方向和 *X*–*Y* 方向的烧结收缩率

Fig. 8　Sintering shrinkage in the *Z* direction and *X*–*Y* direction of the samples

图 8 为经 1 100 ℃烧结 2 h 制备的四种固相含量的 PZT 陶瓷圆片的收缩率。由图 8 可见，随着 PZT 陶瓷粉体固相含量的增加，PZT 陶瓷 *Z* 方向与 *X*–*Y* 方向的线收缩率均减少，*Z* 方向收缩率由 27.93%下降至 20.52%，*X*–*Y* 方向收缩率由 27.13%下降至 20.31%，且 *Z* 方向的收缩率均高于 *X*–*Y* 方向。这是由 FDM 成型技术分层累积导致的，在成型过程中，层与层之间的结合程度弱于同一打印平面内相邻路径间的结合程度，所以 PZT 陶瓷颗粒在烧结过程中在径向方向上所需的移动空间也少于轴向方向。

图 9 为 87%固相含量耗材制备的样品在各阶段的显微形貌图。由图 9a 可以看出，有机物黏结剂在生坯中起到了粘结 PZT 粉体的作用，并使之得以塑形；溶剂脱脂处理后如图 9b，内部 PZT 颗粒间出现了孔隙，颗粒间还可以观察到纤维状细丝的存在；高温脱脂处理后如图 9c 有机物黏结剂在高温下挥发从坯体中排出，PZT 粉体间出现均匀间隙。由图 9d 可见，烧结样品内部的孔隙减少，结合致密，晶粒尺寸较为均匀，说明溶解脱脂+高温脱脂的两步脱脂处理工艺较好地排除了坯体内部的有机物黏结剂，晶粒在烧结过程中逐渐生长结合填充了有机物挥发产生的间隙。

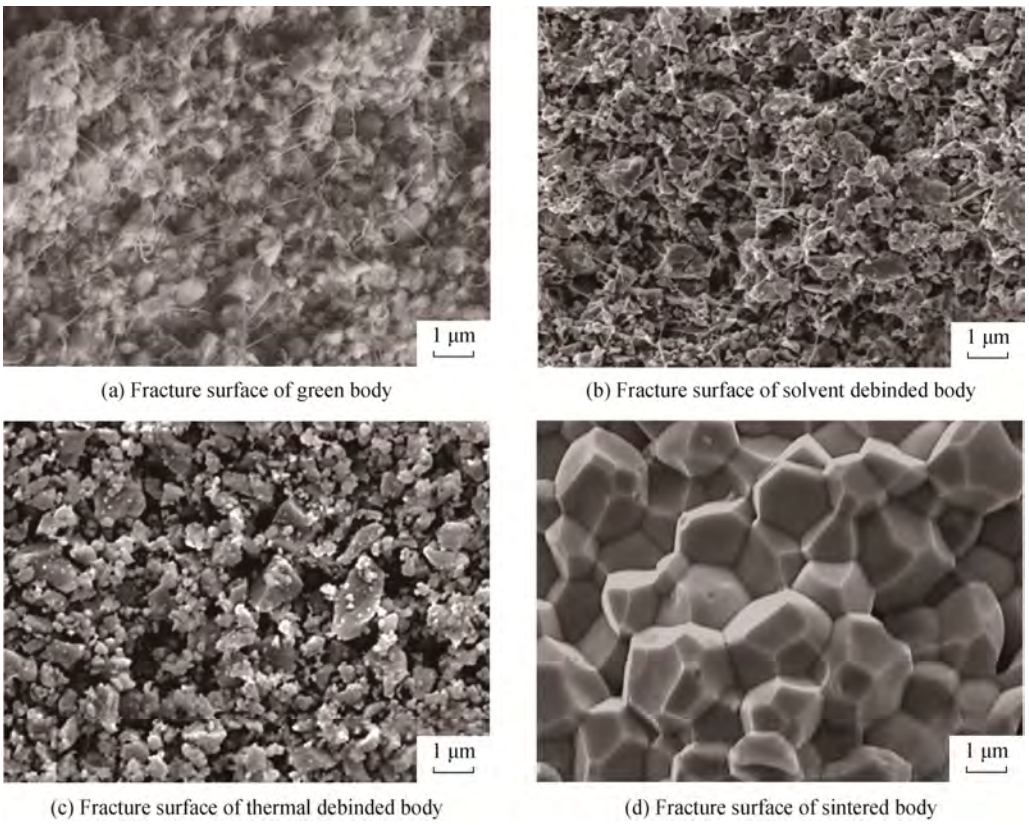

图 9　PZT 样品在各阶段的 SEM 照片

Fig. 9　SEM images of PZT samples in various stages

图 10 为 FDM 打印制备的 87%PZT 压电陶瓷复杂形状构件实物图。由图 10 可见，样品烧结前后对比，没有明显形变和开裂，阵元与薄壁间间隔清晰，验证了 FDM 技术制备 PZT 压电陶瓷复杂形状构件的基本可行性。

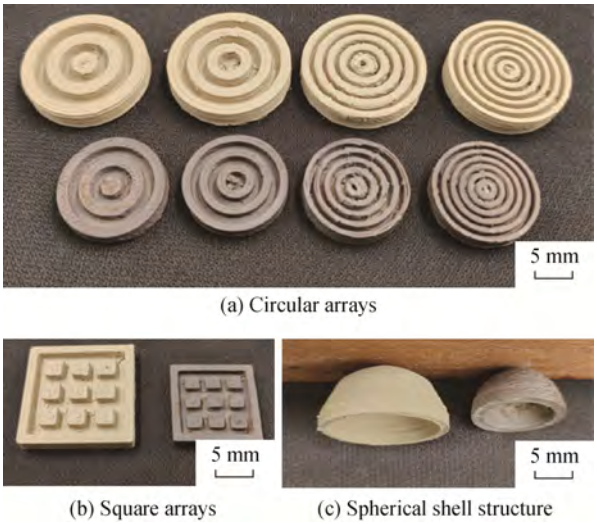

图 10 FDM 制备的 PZT 生坯样品与烧结样品

Fig. 10 Images of green bodies and sintered PZT parts prepared by fused deposition modeling (FDM)

2.3 电学性能

用 87% PZT 打印耗材制备了直径 17.5 mm、厚度 1.35 mm 的 PZT 压电陶瓷圆片，并对其进行电学性能测试。图 11 为测得的介电温谱和 *P*–*E* 电滞回线。由图 11a 可见，相对介电常数 ε_r 随着温度的升高，先增大后下降，所有频率显示只有 1 个峰值，此时温度约 300 ℃，即样品的 Curie 温度 T_C。介电损耗 tanδ 在升温过程中先增大，在接近 Curie 温度时，均出现了不同程度的减小，随后继续增大，接近 400 ℃后介电损耗 tanδ 急剧上升，这主要是因为 PZT 压电陶瓷在高温时导电性增加，导致额外的电流流动，发生了漏导。图 11b 为 87 %固相含量样品在室温、测试频率为 10 Hz，最大电场为 30 kV/cm 下测得的 *P*–*E* 电滞回线。由图 11b 可以看出，电滞回线显示出良好的对称性，但测试曲线不够饱和，呈现“夹持”现象，可能是样品致密度不够高，难以加上较高的测试电压。矫顽场强 E_c 和剩余极化强度 P_r 随着电场的增加而增大，说明在较高的电场作用下电畴转向更容易。可以图中看出，30 kV/cm 时，剩余极化强度 P_r=3.66 μC/cm^2，矫顽场 E_c=7.57 kV/cm。

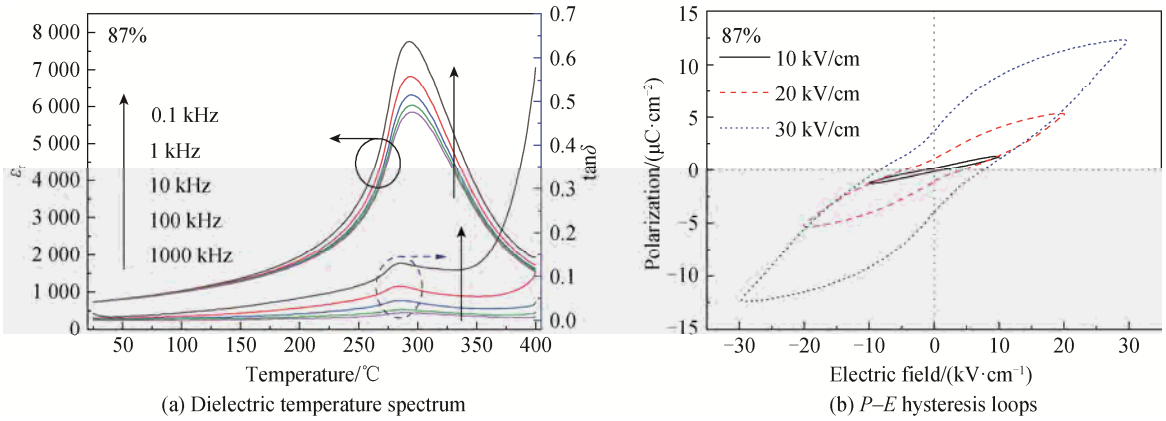

ε_r is dielectric constant; tanδ is dielectric loss.

图 11 10 kHz 频率测得的介电温谱–介电损耗与 *P*–*E* 电滞回线

Fig. 11 Dielectric temperature spectrum measured at 10 kHz and polarization–electric field (*P*–*E*) hysteresis loops

表 1 为不同增材制造技术制备 PZT 压电陶瓷的电学性能，FDM 制备 PZT 压电陶瓷的相对介电常数 ε_r 和介电损耗 tanδ 取 10 kHz 下测试的数据，剩余极化强度 P_r 和矫顽场 E_c 的测试电场强度为

表 1 增材制造 PZT 压电陶瓷电学性能对比

Table 1 Comparison of electrical properties of PZT piezoceramics formed by additive manufacturing

AM techniques	Solid loading	T_C/℃	ε_r	tanδ/%	P_r/(μC·cm^{-2})	E_c/(kV·cm^{-1})	d_{33}/(pC·N^{-1})
FDM	87 wt%	295	724.75	0.334	3.66	7.57	316
DIW[34]	86.21 wt%		1621	3.1			342.6
SLA[35]	78–89 wt%		760–1390	2.0–2.1			212–345
IJP[36]	10 vol%		190	5			

T_C is Curie temperature; P_r is remnant polarization; E_c is coercive electric field; d_{33} is piezoelectric constant.

30 kV/cm。由表 1 可以看出，FDM 制备 PZT 压电陶瓷的压电常数 d_{33} 达到 316 pC/N，与 DIW 和 SLA 制备的 PZT 压电陶瓷相近。而压制成型样品的压电常数 d_{33} 可达 330 pC/N，介电常数 1 450，介电损耗 0.20%，压电常数与介电常数均高于 FDM 成型样品，介电损耗低于 FDM 成型样品，FDM 成型 PZT 压电陶瓷的电学性能较压制样品有所不足，与两者密度的差异相同。

3　结论

1) 采用石蜡有机物黏结剂体系的 PZT 颗粒状混合料在 180 ℃呈现剪切变稀的特性，具备良好的流动性和维形性能，适用于 FDM 成型，且适合制备环形阵列与薄壁结构，成功打印了壁厚 1 mm 的环形阵列、阵元间距最低为 0.25 mm 的矩形阵列和 30°倾角的薄壁结构。

2) FDM 制备的 PZT 陶瓷样品层间结合良好，层间裂隙较少。随着打印耗材固相含量的增加，PZT 陶瓷的密度增大，样品的收缩率降低，且 Z 方向的收缩率均高于 X–Y 方向。固相含量为 87%时，PZT 陶瓷的密度可达 7.82 g/cm^3，达到压制成型样品的 98.49%。

3) 电学性能分析表明，87%固相含量打印耗材制得的 PZT 压电陶瓷 Curie 温度可达 295 ℃，压电常数 d_{33} 达到 316 pC/N，矫顽场 E_c 为 7.57 kV/cm，电学性能稳定，验证了 FDM 制备 PZT 压电陶瓷的可靠性。

参考文献:

[1] CHEN C, WANG X, WANG Y, et al. Additive manufacturing of piezoelectric materials[J]. Adv Funct Materials, 2020, 30(52): 2005141.

[2] CHEN Z Y, SONG X, LEI L W, et al. 3D printing of piezoelectric element for energy focusing and ultrasonic sensing[J]. Nano Energy, 2016, 27: 78–86.

[3] 杨俊涛, 左文建, 张文龙, 等. 压电陶瓷传感器监测混凝土内部缺陷的可行性研究[J]. 硅酸盐通报, 2023, 42(1): 111–122.
YANG Juntao, ZUO Wenjian, ZHANG Wenlong, et al. Bull Chin Ceram Soc, 2023, 42(1): 111–122.

[4] 叶晶晶, 周科朝, 闫明洋, 等. 多孔压电陶瓷压力传感器的制备及性能[J]. 硅酸盐学报, 2023, 51(3): 738–749.
YE Jingjing, ZHOU Kechao, YAN Mingyang, et al. J Chin Ceram Soc, 2023, 51(3): 738–749.

[5] 姚方周, 吴超峰, 李敬锋, 等. 面向应用的(K, Na)NbO_3 基无铅压电陶瓷研究进展[J]. 硅酸盐学报, 2022, 50(3): 587–597.
YAO Fangzhou, WU Chaofeng, LI Jingfeng, et al. J Chin Ceram Soc, 2022, 50(3): 587–597.

[6] 王丹钰, 王安玖, 王五松, 等. 高温压电陶瓷材料的研究进展及应用[J]. 陶瓷学报, 2021, 42(3): 376–388.
WANG Danyu, WANG Anjiu, WANG Wusong, et al. J Ceram, 2021, 42(3): 376–388.

[7] BOUMCHEDDA K, HAMADI M, FANTOZZI G. Properties of a hydrophone produced with porous PZT ceramic[J]. J Eur Ceram Soc, 2007, 27(13–15): 4169–4171.

[8] OKAYASU M, WATANABE K. Precise analysis of compressive strain effects on electric power generation properties of a lead zirconate titanate piezoelectric ceramic[J]. J Adv Ceram, 2016, 5(1): 35–39.

[9] 闫锋, 邬正利, 王文林. 大位移量、高弹性模量压电陶瓷材料的制备与研究[J]. 硅酸盐通报, 2015, 34(4): 1175–1179.
YAN Feng, HUAN Zhengli, WANG Wenlin. Bull Chin Ceram Soc, 2015, 34(4): 1175–1179.

[10] 杨帅, 王明文, 吴杰, 等. 铅基织构压电陶瓷研究进展[J]. 硅酸盐学报, 2022, 50(3): 598–607.
YANG Shuai, WANG Mingwen, WU Jie, et al. J Chin Ceram Soc, 2022, 50(3): 598–607.

[11] YUNUS D E, HE R, SHI W T, et al. Short fiber reinforced 3d printed ceramic composite with shear induced alignment[J]. Ceram Int, 2017, 43(15): 11766–11772.

[12] KORUZA J, BELL A J, FRÖMLING T, et al. Requirements for the transfer of lead-free piezoceramics into application[J]. J Materiomics, 2018, 4(1): 13–26.

[13] CHENG J, CHEN Y, WU J W, et al. 3D printing of $BaTiO_3$ piezoelectric ceramics for a focused ultrasonic array[J]. Sensors, 2019, 19(19): 4078.

[14] CUI H C, HENSLEIGH R, YAO D S, et al. Three-dimensional printing of piezoelectric materials with designed anisotropy and directional response[J]. Nat Mater, 2019, 18(3): 234–241.

[15] LIU K, SUN H J, TAN Y L, et al. Additive manufacturing of traditional ceramic powder via selective laser sintering with cold isostatic pressing[J]. Int J Adv Manuf Technol, 2017, 90(1): 945–952.

[16] LEE J H, HWANG H J, KIM J H, et al. Ceramic ink-jet printing on glass substrate using oleophobic surface treatment[J]. J Korean Ceram Soc, 2016, 53(1): 75–80.

[17] 包秀兰, 陈燕, 吉红伟, 等. 锆钛酸铅压电陶瓷的制备工艺研究[J]. 陶瓷学报, 2019, 40(2): 153–158.
BAO Xiulan, CHEN Yan, JI Hongwei, et al. J Ceram, 2019, 40(2): 153–158.

[18] HU X P, LI X S, YAN K, et al. Fabrication of porous PZT ceramics using micro-stereolithography technology[J]. Ceram Int, 2021, 47(22): 32376–32381.

[19] LIU K, ZHOU C Y, HU J M, et al. Fabrication of Barium titanate ceramics via digital light processing 3D printing by using high refractive index monomer[J]. J Eur Ceram Soc, 2021, 41(12): 5909–5917.

[20] LI Z Y, LI J, LUO H, et al. Direct ink writing of 3D piezoelectric ceramics with complex unsupported structures[J]. J Eur Ceram Soc, 2022, 42(9): 3841–3847.

[21] GIBERTI H, STRANO M, ANNONI M. An innovative machine for Fused Deposition Modeling of metals and advanced ceramics[J]. MATEC Web Conf, 2016, 43: 03003.

[22] CHEN Z W, LI Z Y, LI J J, et al. 3D printing of ceramics: A review[J]. J Eur Ceram Soc, 2019, 39(4): 661–687.

[23] DECKERS J, MEYERS S, KRUTH J P, et al. Direct selective laser sintering/melting of high density alumina powder layers at elevated temperatures[J]. Phys Procedia, 2014, 56: 117–124.

[24] WANG M, XIE C, HE R J, et al. Corrections to: Polymer-derived silicon nitride ceramics by digital light processing based additive manufacturing[J]. J Am Ceram Soc, 2019, 102(12): 7769–7770.
[25] KRINITCYN M, FU Z W, HARRIS J, et al. Laminated object manufacturing of *in-situ* synthesized MAX-phase composites[J]. Ceram Int, 2017, 43(12): 9241–9245.
[26] XIE H H, YANG X F, LIU P, et al. 3D gel printing of alumina ceramics followed by efficient multi-step liquid desiccant drying[J]. J Eur Ceram Soc, 2021, 41(13): 6634–6640.
[27] ONAGORUWA S, BOSE S, BANDYOPADHYAY A. Fused deposition of ceramics (FDC) and composites[J]. Proc Solid Free Fabr Symp, 2001: 224–231.
[28] HE Q L, JIANG J, YANG X F, et al. Additive manufacturing of dense zirconia ceramics by fused deposition modeling via screw extrusion[J]. J Eur Ceram Soc, 2021, 41(1): 1033–1040.
[29] 张力, 杨现锋, 徐协文, 等. 熔融沉积法 3D 打印制备氧化锆陶瓷及其力学性能研究[J]. 无机材料学报, 2021, 36(4): 436–442.
ZHANG Li, YANG Xianfeng, XU Xiewen, et al. J Inorg Mater, 2021, 36(4): 436–442.
[30] LOUS G M, CORNEJO I A, MCNULTY T F, et al. Fabrication of Piezoelectric Ceramic/Polymer Composite Transducers using Fused Deposition of Ceramics[J]. MRS Online Proc Libr, 1998, 542(1): 105–110.
[31] KOŠIR T, SLAVIČ J. Single-process fused filament fabrication 3D-printed high-sensitivity dynamic piezoelectric sensor[J]. Addit Manuf, 2022, 49: 102482.
[32] KIM H, ISLAM M T, MD DIDARUL I, et al. Increased piezoelectric response in functional nanocomposites through multiwall carbon nanotube interface and fused-deposition modeling three-dimensional printing[J]. MRS Commun, 2017, 7(4): 960–966.
[33] TAO R, SHI J H, GRANIER F, et al. Multi-material fused filament fabrication of flexible 3D piezoelectric nanocomposite lattices for pressure sensing and energy harvesting applications[J]. Appl Mater Today, 2022, 29: 101596.
[34] LIU K, XIA Y H, ZHANG Q Q, et al. Effect of the slurry composition on the piezoelectric properties of PZT ceramics fabricated via materials extrusion 3D printing[J]. Ceram Int, 2023, 49(12): 20024–20033.
[35] CHEN Y, BAO X L, WONG C M, et al. PZT ceramics fabricated based on stereolithography for an ultrasound transducer array application[J]. Ceram Int, 2018, 44(18): 22725–22730.
[36] KUSCER D, DRNOVŠEK S, LEVASSORT F. Inkjet-printing-derived lead-zirconate-titanate-based thick films for printed electronics[J]. Mater Des, 2021, 198: 109324.

Additive Manufacturing of Lead Zirconate Titanate Piezoelectric Ceramic by Fused Deposition Modeling

LIU Yueming[1], *DONG Haolin*[1], *LIU Peng*[1], *YANG Xianfeng*[1], *ZHAO Wei*[2], *XIE Zhipeng*[3]
(1. Changsha University of Science & Technology, College of Materials Science and Engineering, Changsha 410114, China;
2. Tianjin Chengjian University, School of Materials Science and Engineering, Tianjin 300384, China;
3. State Key Laboratory of New Ceramic and Fine Processing, School of Materials Science and Engineering, Tsinghua University, Beijing 100083, China)

Extended Abstract

Introduction Lead zirconate titanate (PZT) piezoelectric ceramics are widely used in electronic components. With the continuous development of intelligent, integrated and lightweight piezoelectric devices, the shape and structure of piezoelectric ceramic components become more complex. 3D printing technology has potential advantages in the personalized manufacturing of complex ceramic parts, especially the fused deposition modeling (FDM) method, which has the advantages of high efficiency, low cost, and wide material adaptability. This paper was to prepare PZT piezoelectric ceramics by FDM. In addition, the process optimization, printing performance, sintering behavior, and electrical properties were also investigated.

Methods A PZT powder with an average particle size of 2.85 μm was used. An organic binder was composed of 58% paraffin wax (PW, purity: 99% in mass fraction, the same below), 5% stearic acid (SA, 98%), 20% Polyethylene (PE, 99%), and 17% ethylene-vinyl acetate copolymer (EVA, 98%). The ceramic powder and organic binder were thoroughly mixed by a double-roller mixing machine at 130 ℃ for 60 min, and then crushed into granules of less than 5 mm. The solid loading of the feedstock was set to 83%, 85%, 87%, and 89%. A commercial extrusion printer (UP-R200, Shenzhen Uprise 3D Technology Co., Ltd., China) with the extrusion nozzle diameter of 0.5 mm, and the layer thickness of 0.2 mm for FDM was used in this study. The printing condition was printing temperature of 120 ℃, print speed of 40 mm/s, and printing platform temperature of 85 ℃. Some complex shaped parts like ring array, rectangular array, and thin-walled cylindrical structures were printed. The printed green bodies were firstly placed in kerosene for solvent debinding at 40 ℃ for 20 h and then dried in an oven at 40 ℃ for 15 h. The dried parts were heated at 600 ℃ for 2 h. After thermal debinding, the samples were put into a crucible with a lid, buried on PZT powder, and sintered in the furnace at 1 100 ℃ for 2 h. The PZT ceramics coated with silver electrodes were polarized in an electric field of 2.5 kV/mm in silicone oil at 120 ℃ for 20 min. The phase composition and structure of the sample were determined by a model D8 Advance X-ray diffractometer (XRD, Germany) with detect angles ranging from 10° to 80°. The rheological properties of the printing consumables were tested at 180 ℃ by a model Rosand RH2000 capillary rheometer (Malvern Co., UK). The microstructures of samples were analyzed by a model JSM-6700F field emission scanning electron microscope (SEM, JEOL Co., Japan). The density of the samples was measured

by a drainage method. The dielectric constant ε_r and dielectric loss δ were measured by a model Agilent-4294A impedance analyzer (USA). The ferroelectric properties were analyzed by a model aix ACCT-TF Analyzer 2000 ferroelectric tester (Germany). The piezoelectric constant of the polarized sample was measured by a model ZJ-3AN quasi-static d_{33} meter (Institute of Acoustics, Chinese Academy of Sciences, China).

Results and discussion At a constant solid loading, the shear viscosity of the feedstock at 180 ℃ decreases with the increase of shear rate, and has obvious shear thinning characteristics, which is beneficial to the extrusion process. At a constant shear rate, the higher the solid loading is, the higher the measured shear viscosity will be. At a shear rate of 100 s^{-1}, the shear viscosity is 30.30, 45.07, 47.08 Pa·s and 655.21 Pa·s respectively as the solid loading increases. Annular arrays with a wall thickness of 1 mm, rectangular arrays with an element spacing of 0.25 mm, and annular thin-wall blank samples with an inclination angle of 30° are printed, indicating that the prepared feedstock has a good printing performance. The SEM images show that the prepared PZT ceramic samples have a good interlayer bonding. Each layer is straight, uniform and continuous. After debinding and sintering, the interior of the material is uniform and dense without obvious pore defects, which shows that PZT ceramics with a good interlayer bonding can be obtained by the FDM method. The density of both green body and sintered body increases with the increase of solid loading, and the density of sintered body increases from 7.55 g/cm^3 to 7.84 g/cm^3. The results show that the sintering shrinkage in the Z direction is higher than that in the *X*–*Y* direction. The SEM images of PZT samples at each stage show that the two-step debinding process of solvent debinding + thermal debinding is beneficial to eliminating organic binders without causing defects. PZT piezoelectric ceramic sheets with a diameter of 17.5 mm and a thickness of 1.35 mm are prepared using a feedstock with a solid loading of 87%. The electrical property analysis indicates that the Curie temperature reaches 295℃, the coercive electric field *E* is 7.57 kV/cm, the remnant polarization P_r reaches 3.66 μC/cm^2, and the piezoelectric constant d_{33} reaches 316 pC/N.

Conclusions The prepared feedstock with a high solid content and a low viscosity exhibited a typical shear thinning rheology and an excellent printing performance. A PZT spherical shell structure without support was prepared. The PZT ceramic samples had good interlayer bonding and no interlayer cracks. The density of PZT ceramics increased with increasing the solid loading. At a solid loading of 87%, the density of PZT ceramic reached 7.82 g/cm^3, and the piezoelectric constant d_{33} was 316 pC/N. This study provided an effective approach for the preparation of complex structure PZT piezoelectric ceramics.

Keywords 3D printing; lead zirconate titanate; fused deposition modeling; piezoelectric ceramic